Lab on a Chip

Dynamic Article Links

Cite this: *Lab Chip*, 2011, **11**, 1770

www.rsc.org/loc

PAPER

Hybrid electrokinetic manipulation in high-conductivity media†

Jian Gao,[ab] Mandy L. Y. Sin,[a] Tingting Liu,[a] Vincent Gau,[c] Joseph C. Liao[d] and Pak Kin Wong*[a]

Received 19th January 2011, Accepted 25th March 2011
DOI: 10.1039/c1lc20054b

This study reports a hybrid electrokinetic technique for label-free manipulation of pathogenic bacteria in biological samples toward medical diagnostic applications. While most electrokinetic techniques only function in low-conductivity buffers, hybrid electrokinetics enables effective operation in high-conductivity samples, such as physiological fluids (~1 S m^{-1}). The hybrid electrokinetic technique combines short-range electrophoresis and dielectrophoresis, and long-range AC electrothermal flow to improve its effectiveness. The major technical hurdle of electrode instability for manipulating high conductivity samples is tackled by using a Ti–Au–Ti sandwich electrode and a 3-parallel-electrode configuration is designed for continuous isolation of bacteria. The device operates directly with biological samples including urine and buffy coats. We show that pathogenic bacteria and biowarfare agents can be concentrated for over 3 orders of magnitude using hybrid electrokinetics.

Introduction

Microfluidics has been touted as the transformative technology for numerous biochemical applications, such as single cell analysis and point-of-care testing.[1–3] Despite the fact that intensive efforts have been devoted to the field, microfluidics has not yet been widely used and transforming microfluidic biosensing systems from research to reality remains an elusive goal.[4,5] Arguably, the applicability of the microfluidic sensing systems is ultimately limited by the world-to-chip interface problem and the matrix effect.[6–10] The matrix effect is defined as the effect of nonspecific components in the samples, such as metabolities, cells, proteins, and salts present in biological samples. The matrix effect can significantly limit the accuracy and reproducibility of a microfluidic sensing system and represents a fundamental challenge in using microfluidics for biochemical and clinical applications. On the other hand, the world-to-chip interface problem is a result of the small sample volume in microfluidics. Considering a pathogen sensor for detecting a sample with 1000 cfu/ml, there is on average less than 1 target pathogen in the typical volume of a microfluidic system (nl to μl). Innovative techniques for on-chip sample manipulation, such as preconcentration and isolation, are required for addressing the matrix effect and world-to-chip interface to realize the potential of lab-on-a-chip systems.[5,11]

Electrokinetics has been one of the most powerful approaches for microfluidic manipulation. Electrokinetic techniques, including electrophoresis (EP),[12] dielectrophoresis (DEP),[13] and AC electrothermal flow (ACEF)[14,15] are ideal methods for manipulating nanoscale and biological objects, such as cells and molecules, due to the length scale matching for effective momentum coupling, label-free operation, simple fabrication processes, and small voltage requirements.[16–28] For instance, EP describes the translational movement of charged particles in a liquid medium under an external electric field. When a particle with charge q is under a steady electric field E, the particle experiences an electrostatic force F_{EP}.

$$F_{EP} = Eq \quad (1)$$

In addition to EP, DEP is another particle force that acts directly on a particle, such as a bacterium, and is highly effective for short-range manipulation of particles. During DEP manipulation, a dipole is induced in a polarizable particle when the particle is subjected to an electric field. If the electric field is nonuniform, the particle experiences a net force toward the high or low electric field region. The time averaged dielectrophoretic force is given by

$$F_{DEP} = 2\pi R^3 \varepsilon \mathrm{Re}[K(\omega)]\nabla|E_{rms}|^2 \quad (2)$$

where R is the particle radius, ε is the permittivity of the medium, E_{rms} is the root-mean-square electric field, ω is the angular frequency, and $\mathrm{Re}[K(\omega)]$ represents the effective polarizability of the particle in the medium. DEP is especially effective near the edge of the electrode and decays rapidly away from the electrode due to its dependence on the gradient of the square of the electric

[a]*Department of Aerospace and Mechanical Engineering, University of Arizona, Tucson, Arizona, 85721, USA. E-mail: pak@email.arizona.edu; Fax: +1-520-621-8191; Tel: +1-520-626-2215*
[b]*Department of Chemical Engineering, Shandong Polytechnic University, Jinan, 250353, China*
[c]*GeneFluidics Inc, Monterey Park, California, 91754, USA*
[d]*Department of Urology, Stanford University, Palo Alto, California, 94304, USA*

† Electronic supplementary information (ESI) available: Videos of the hybrid electrokinetic concentration processes under static and dynamic conditions. See DOI: 10.1039/c1lc20054b

field, ∇E^2_{rms}. Manipulation of physiological samples (*e.g.*, urine) based on DEP alone is often a challenging task.[29] On the other hand, ACEF is an electrohydrodynamic effect. ACEF arises from the temperature gradient in a medium generated by joule heating of the fluid. This temperature gradient induces local changes in the conductivity, permittivity, viscosity, and density of the solution. These gradients can generate forces, which act on the fluid. For example, a conductivity gradient produces Coulomb forces while a permittivity gradient produces dielectric forces. An analytical expression of the force generated is given for parallel electrodes.[15,16] The order of magnitude of the force on the fluid is

$$f_{ACEF} = -M(\omega, T)\left(\frac{\varepsilon\sigma V_{rms}^4}{2k\pi^3 r^3 T}\right)\left(1 - \frac{2\phi}{\pi}\right) \quad (3)$$

with $M(\omega,T)$ being

$$M(\omega, T) = \left(\frac{\frac{T\partial\sigma}{\sigma\partial T} - \frac{T\partial\varepsilon}{\varepsilon\partial T}}{1 + (\omega\tau)^2} + \frac{1}{2}\frac{T}{\varepsilon}\frac{\partial\varepsilon}{\partial T}\right) \quad (4)$$

where σ is the conductivity of the medium, V_{rms} is the root-mean-squre voltage, T is the temperature, and r and ϕ are the polar coordinates with reference to the middle of the electrode gap. k is the thermal conductivity. $M(\omega,T)$ is a dimensionless factor describing the variation of the electrothermal force as a function of applied frequency. τ is the charge relaxation time. ACEF is highly effective for manipulating fluids with high conductivities and the applied voltage and frequency are effective parameters for adjusting the strength of ACEF. Typically, only a small temperature rise, *e.g.*, a few degrees, is required for generating fluid motion and the temperature rise can be approximated by[14–16]

$$\Delta T = \frac{\sigma V^2}{k} \quad (5)$$

While electrokinetics is promising for addressing the major challenges of microfluidic sensing systems, its applicability in biochemical applications is limited by the ineffectiveness of most electrokinetic effects in high conductivity buffers, the short-range effects of DEP, and the instability of microelectrodes under large driving voltages.[29–31]

Herein, we describe a hybrid electrokinetic process, which combines EP, DEP, and ACEF for label-free sample manipulation in microfluidic systems. ACEF, which is especially effective in high-conductivity buffers and has long-range hydrodynamic effects, is combined with EP and DEP to overcome the short-range effect of these electrokinetic techniques and enhance their effectiveness in high-conductivity buffers.[32–34] While most electrokinetic techniques only function in low-conductivity buffers, hybrid electrokinetics enables effective manipulation of biological objects in high-conductivity samples (1 S m^{-1}), which are comparable to physiological fluids and biological buffers. Using a 3-parallel-electrode design with a Ti–Au–Ti sandwich electrode configuration, we demonstrate that pathogenic bacteria and biological warfare simulants can be concentrated by 2–3 orders of magnitude in high conductivity media (on the order of 1 S m^{-1}) including urine and buffy coat samples.

Experimental methods

Microfluidic device

The electrode configuration for pathogen manipulation is shown in Fig. 1 a–c. The device consisted of 8 sets of 3-parallel-electrodes arranged in series and was fabricated by sputtering 150 nm titanium, 300 nm gold and 150 nm titanium on a glass substrate. The electrodes were patterned by lift-off. The length, width and distance of each electrode were 2.5 mm, 30 μm and 15 μm respectively. The distance between each pair of electrodes was 0.5 mm. The microfluidic chip was fabricated by polydimethylsiloxane (PDMS) molding.[35] The glass substrate with microelectrodes was sealed with the PDMS microchannel by plasma treatment. The fluid flow in the dynamic experiment was generated by a programmable syringe pump (NE-100, New Era Pump Systems, Inc. USA). A function generator (Hewlett Packard, 33120A) was used to supply the voltage signals (both AC and DC-bias).

Pathogens and physiological samples

The pathogenic *Escherichia coli* (*E. coli*) was isolated as part of a research protocol approved by the Stanford University Institutional Review Board. *Acinetobacter baumannii* (*A. baumannii*) and *Bacillus globigii* (*B. globigii*) were purchased from ATCC (BAA-1710; 49822, USA). Bacteria were cultured to 10^9 cfu/ml and pre-stained using 3,3′-dihexyloxacarbocyanine iodide ($DiOC_6(3)$, Sigma).[36] The samples were diluted to appropriate concentrations using Tris-acetate-EDTA (TAE, Sigma, USA) buffer before the experiment. The buffy coats from human blood samples were purchased from Innovative Research Company, USA.

Data collection and analysis

The electrokinetic chip was loaded onto a digital inverted epi-fluorescence microscope (DMI 4000B, Leica Microsystems). Samples were illuminated at a wavelength of 480 ± 40 nm with a mercury lamp, and images were recorded at 527 ± 30 nm. All experiments were performed at room temperature. The dynamic processes of bacteria concentration were recorded by a CCD camera and directly digitized into a video capture system. The images and videos were processed by NIH ImageJ software. The imaging and data analysis processes were performed using our published procedure.[37] Fluorescence intensity was normalized by the initial value before the application of the driving signal. Therefore, the normalized intensity represents the increase in concentration of the sample. Data of bacteria kinetics were smoothed out by weighted averages with nearest neighbours.[37] The temperature near the work electrodes was experimentally measured using a microscale two-color fluorescence thermometry technique.[38]

Results and discussion

Pathogen concentration using hybrid electrokinetics

The 3-parallel-electrode design of the hybrid electrokinetic processor is shown in Fig. 1a–b. In this design, ACEF entrains target cells far away from the bulk solution toward the electrode

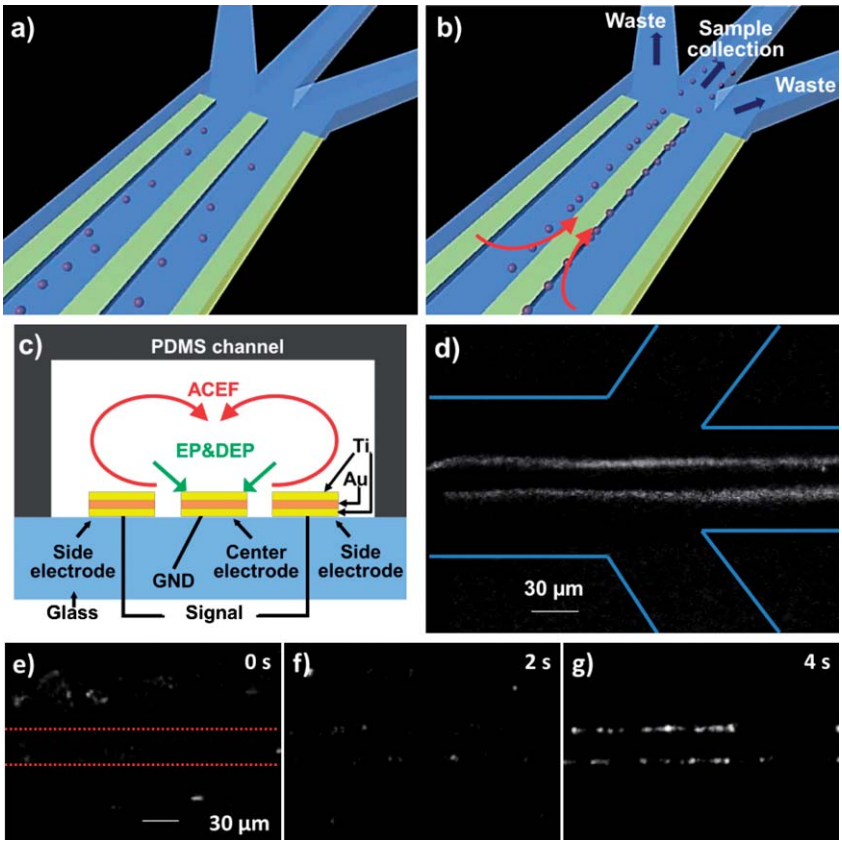

Fig. 1 A hybrid electrokinetic device for manipulating biological objects. a) Bacteria randomly distributed before the application of the electric field. b) Bacteria are concentrated on the edges of the center electrode by hybrid electrokinetics and can be delivered to the sample collection channel. c) Ti–Au–Ti electrodes integrated in a microfluidic channel for hybrid electrokinetic manipulation. d) *E. coli* fluorescently labeled with $DiOC_6(3)$ are collected by the channel downstream under dynamic conditions. Lines indicate the channel boundaries. e), f), g) Video time series illustrating the hybrid electrokinetic concentration process of pathogenic *E. coli*. Dotted lines in e) indicate the center electrode. The applied voltage is 2 Vpp at 2 MHz with 1.5 V DC offset.

surface, where DEP is most effective. Target cells can then be trapped on the edges of the central electrode by DEP and EP, and delivered to the sample collection channel with continuous fluid flow. The long range fluid flow allows DEP to be effective in high conductivity buffers and dramatically enhances the effective range of target manipulation (Fig. 1c). In the experiment, the effective capture region was over 500 μm while the 3-parallel-electrode dimension was only 120 μm in width. The fluid flow also significantly reduces the driving voltage to only a few volts for manipulating biological objects. In addition, we tested the stability of several metal electrodes for hybrid electrokinetic manipulation in high conductivity media and identified a multi-layer Ti–Au–Ti electrode which exhibited the best stability (Fig. 1c). The sandwich Ti–Au–Ti structure can endure high voltages for an extended period of time without observable bubble formation or deterioration of the electrodes, which is conceivably a result of the thin oxidized film on titanium. The stability is essential for electrokinetic manipulation in high conductivity media.

E. coli clinical isolates spiked in high conductivity media, including buffers, urine samples, and buffy coats, were applied as model systems for studying the governing dynamics of hybrid electrokinetics. During the experiment, the bacteria were rapidly focused on the edges of the center electrode. Under dynamic conditions (with flow), the bacteria were entrained with the flow and collected continuously by the sample collection channel at high flow rates (Fig. 1d). Under static conditions (no flow), the bacteria could be trapped near the electrode edges in a few seconds and continued to aggregate at the edges due to dipole–dipole interactions (Fig. 1e–g). The temperature rise induced by hybrid electrokinetics does not introduce any observable damages to the bacteria in our experimental conditions and the bacteria remain active after the removal of the electric field. Applying 5 V peak-to-peak at 1 MHz to a sample with conductivity 1 S m^{-1}, the temperature was experimentally determined to be 36 °C using two-color fluorescence thermometry. This value is in reasonable agreement with 32 °C estimated using eqn (5).

Characterisitcs of hybrid electrokientics

To investigate hybrid electrokinetics, the effects of frequency, DC offset, voltage, and buffer conductivity on bacterial concentration were systematically studied under static conditions. Fig. 2a shows the concentration processes at frequencies from 300 kHz to 10 MHz. Fig. 2b shows the frequency dependence of the intensity, *i.e.*, the concentration of *E. coli*, after 120 s of electrokinetic concentration. Lower frequencies were not

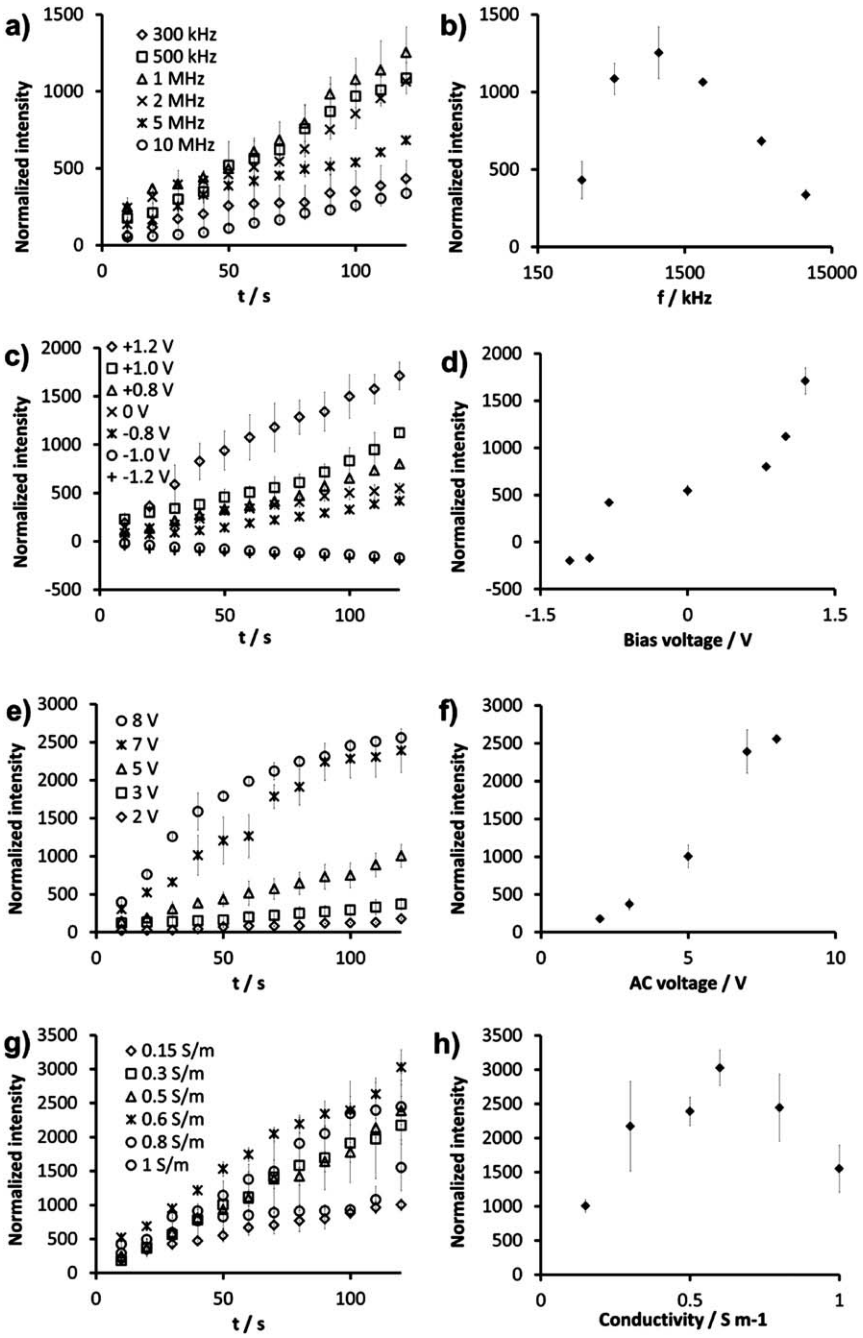

Fig. 2 (a,c,e,g) Dependence of the concentration effects on the applied frequency (a), DC offset (c), AC voltage (e), and buffer conductivity (g). (b,d,f,h) Intensity values after 120 s. The intensity values are normalized by the initial value. Unless specified otherwise, the applied frequency, DC offset, AC voltage and conductivity are 1 MHz, 1 V, 5 V. and 0.15 S m^{-1}, respectively.

tested to avoid formation of bubbles. The local concentration of the bacteria could be increased by over 3 orders of magnitude and was maximized at 1 MHz. It should be noted that ACEF is independent of the applied frequency in the range tested (300 kHz to 10 MHz).[32] For a sample of 0.15 S m^{-1}, the charge relaxation frequency is approximately 34 MHz. This indicates that the observed frequency dependence of hybrid electrokinetics is mainly contributed by DEP, which is sensitive to the applied frequency in this condition (Fig. 2a–b). In fact, the polarizability of *E. coli* has been reported to maximize at 1 MHz,[39] which further supports that the frequency dependence of hybrid electrokinetics is dominated by DEP in this condition. Fig. 2c–d shows the dependence of DC offset on the *E. coli* concentration. The concentration effect of hybrid electrokinetics increases linearly with the DC offset, which creates a time average non-zero electrophoretic force on the bacteria. Negative values indicated accumulation of bacteria in the side electrode. The crossover voltage for this transition occurred between −0.8 V to −1 V. The intensity value without DC offset was approximately 30% of the value X with a 1.2 V DC offset. This demonstrates the

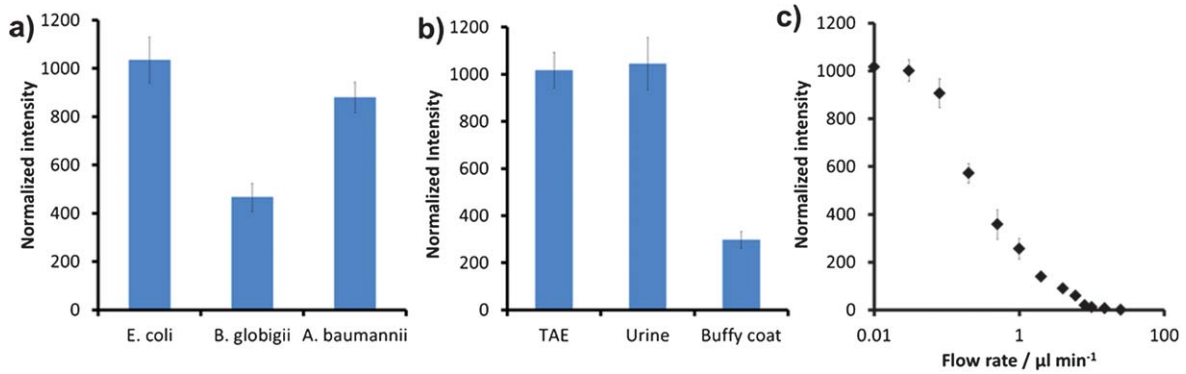

Fig. 3 a) Concentration efficiencies of *E. coli*, *A. baumannii*, and *B. globigii* in TAE buffer. b) Concentration efficiencies of *E. coli* in TAE buffer (1.0 S m^{-1}), human urine (2.3 S m^{-1}) and buffy coat (1.2 S m^{-1}). c) Dependence of the concentration effects of pathogenic *E. coli* on the flow rate. Data represent the intensity after applying 5 V peak-to-peak at 1 MHz with a 1.0 V DC offset for 120 s.

involvement of EP in hybrid electrokinetics. However, a DC potential alone is unable to concentrate the bacteria due to electrode polarization. Fig. 2e–f shows the dependence of the AC driving voltage. The dependence of the intensity on the voltage after 120 s showed a power exponent of 1.990 ± 0.144. Since DEP is proportional to the square of the applied voltage, the data suggest the trapping of bacteria is contributed by DEP. Remarkably, the voltage dependency of the initial rate (first 20 s) of the concentration displayed a power exponent of 3.72 ± 0.144. This indicates the initial concentration process is dominated by ACEF, which has a fourth power dependence on the applied voltage. Fig. 2g–h shows the conductivity dependence of hybrid electrokinetics. In general, the concentration process was effective in the range of 0.1 to 1 S m^{-1} and maximizes at 0.6 S m^{-1}. Collectively, our data reveal that the long-range ACEF transports target bacteria from far away to the region near the electrode surface, where they are trapped by a combination of EP and DEP.

Hybrid electrokinetic manipulation of physiological samples

In addition to pathogenic *E. coli*, we have also demonstrated hybrid electrokinetics for manipulating other bacteria and biological warfare simulants including *A. baumannii* and *B. globigii*. Fig. 3a compares the concentration effects in TAE buffers (1 S m^{-1}). In general, the result shows that hybrid electrokinetics is capable of manipulating different bacteria. The concentration efficiency for *A. baumannii* was comparable to *E. coli* and the value for *B. globigii* was 50% lower. The difference in concentration efficiency for *B. globigii* can be understood by the intrinsic differences in the size, polarizability, and charge between different bacteria. To demonstrate the applicability of hybrid electrokinetics in physiological fluids, we spiked pathogenic *E. coli* into urine and buffy coats and tested the concentration efficiencies (Fig. 3b). The efficiency with TAE buffer and urine were 3-fold higher than with buffy coats. This could be contributed by the higher viscosity of buffy coats and the different conductivities. Nevertheless, the concentration of *E. coli* can be increased by over 2 orders of magnitude in buffy coats. Fig. 3c shows the concentration efficiency in dynamic conditions with different flow rates. There is a trade-off between the throughput and the concentration efficiency at high flow rates. Below 0.1 µl min^{-1}, the bacteria were trapped at the edges similar to the static condition. The bacteria could be eluted out by removing the electric potential. This allowed continuous isolation of the target from the sample matrix and pre-concentration of the target pathogens for downstream processing.

Conclusions

In summary, we have demonstrated a hybrid electrokinetic technique that enables AC electrokinetic manipulation of biological entities in physiological samples. The technique addresses the two major hurdles of microfluidic systems including the matrix effect and the world-to-chip interface problem. The inclusion of electrothermal flow has significantly increased the efficiency and applicability of the hybrid electrokinetic technique. Using the 3-parallel-electrode design with the Ti–Au–Ti configuration, we have successfully demonstrated the manipulation of various bacteria in physiological samples. Since the final trapping efficiency is mainly contributed by DEP, the platform maintains the selectivity of DEP separation. In addition, the technology can be combined with optical or electrochemical detection platforms for molecular and phenotyping analyses of infectious agents.[40–43] With the effectiveness and applicability of hybrid electrokinetics, we envision that in the future this platform will be further expanded for other biomedical applications, such as capturing exfoliated bladder cancer cells in urine and circulating tumor cells in blood.

Acknowledgements

This work is supported by NIH Director's New Innovator Award (1DP2OD007161-01), NIH NIAID (1U01AI082457-01; R43AI088756-01), NIH NICHD (R43HD065303-01), NSF (0930900; 0900899), NSFC (20805027) and SDNSF (Q2007B04, Y2008B39).

Notes and references

1 Y. Pan, G. A. Sonn, M. L. Sin, K. E. Mach, M. C. Shih, V. Gau, P. K. Wong and J. C. Liao, *Biosens. Bioelectron.*, 2010, **26**, 649–654.
2 C. H. Chen, Y. Lu, M. L. Y. Sin, K. E. Mach, D. D. Zhang, V. Gau, J. C. Liao and P. K. Wong, *Anal. Chem.*, 2010, **82**, 1012–1019.
3 N. Li and P. K. Wong, *Bioanalysis*, 2010, **2**, 1689–1699.

4 G. M. Whitesides, *Nature*, 2006, **442**, 368–373.
5 T. H. Wang and P. K. Wong, *J. Assoc. Lab. Autom.*, 2010, **15**, A15–A16.
6 D. Sviridov and G. L. Hortin, *Clin. Chim. Acta*, 2009, **404**, 140–143.
7 M. L. Chiu, W. Lawi, S. T. Snyder, P. K. Wong, J. C. Liao and V. Gau, *J. Assoc. Lab. Autom.*, 2010, **15**, 233–242.
8 R. Mariella, *Biomed. Microdevices*, 2008, **10**, 777–784.
9 J. Wang, *Biosens. Bioelectron.*, 2006, **21**, 1887–1892.
10 S. Choi, M. Goryll, M. L. Y. Sin, P. K. Wong and J. Chae, *Microfluid. Nanofluid.*, 2011, **10**, 231–247.
11 W. Lawi, C. Wiita, S. T. Snyder, F. Wei, D. Wong, P. K. Wong, J. C. Liao, D. A. Haake and V. Gau, *J. Assoc. Lab. Autom.*, 2009, **14**, 407–412.
12 T. B. Jones, *Electromechanics of particles*, Cambridge University Press, Cambridge; New York, 1995.
13 H. A. Pohl, *J. Appl. Phys.*, 1951, **22**, 869–871.
14 N. G. Green, A. Ramos, A. Gonzalez, A. Castellanos and H. Morgan, *J. Electrost.*, 2001, **53**, 71–87.
15 A. Castellanos, A. Ramos, A. Gonzalez, N. G. Green and H. Morgan, *J. Phys. D: Appl. Phys.*, 2003, **36**, 2584–2597.
16 A. Ramos, H. Morgan, N. G. Green and A. Castellanos, *J. Phys. D: Appl. Phys.*, 1998, **31**, 2338–2353.
17 M. P. Hughes, *Nanotechnology*, 2000, **11**, 124–132.
18 P. K. Wong, T. H. Wang, J. H. Deval and C. M. Ho, *IEEE/ASME Trans. Mechatron.*, 2004, **9**, 366–376.
19 W. Y. Ng, S. Goh, Y. C. Lam, C. Yang and I. Rodriguez, *Lab Chip*, 2009, **9**, 802–809.
20 S. Park, M. Koklu and A. Beskok, *Anal. Chem.*, 2009, **81**, 2303–2310.
21 M. L. Y. Sin, V. Gau, J. C. Liao, D. A. Haake and P. K. Wong, *J. Phys. Chem. C*, 2009, **113**, 6561–6565.
22 M. Koklu, S. Park, S. D. Pillai and A. Beskok, *Biomicrofluidics*, 2010, **4**, 034107.
23 J. E. Gordon, Z. Gagnon and H. C. Chang, *Biomicrofluidics*, 2007, **1**, 44102.
24 Z. R. Gagnon and H. C. Chang, *Appl. Phys. Lett.*, 2009, **94**, 024101.
25 Z. Gagnon, J. Mazur and H. C. Chang, *Lab Chip*, 2010, **10**, 718–726.
26 M. Sancho, G. Martinez, S. Munoz, J. L. Sebastian and R. Pethig, *Biomicrofluidics*, 2010, **4**, 022802.
27 R. Pethig, *Biomicrofluidics*, 2010, **4**, 022811.
28 I. F. Cheng, V. E. Froude, Y. Zhu, H. C. Chang and H. C. Chang, *Lab Chip*, 2009, **9**, 3193–3201.
29 R. Krishnan, B. D. Sullivan, R. L. Mifflin, S. C. Esener and M. J. Heller, *Electrophoresis*, 2008, **29**, 1765–1774.
30 H. C. Feldman, M. Sigurdson and C. D. Meinhart, *Lab Chip*, 2007, **7**, 1553–1559.
31 J. Wu, M. Lian and K. Yang, *Appl. Phys. Lett.*, 2007, **90**, 234103.
32 M. L. Y. Sin, V. Gau, J. C. Liao and P. K. Wong, *J. Assoc. Lab. Autom.*, 2010, **15**, 426–432.
33 M. L. Y. Sin, Y. Shimabukuro and P. K. Wong, *Nanotechnology*, 2009, **20**, 165701.
34 P. K. Wong, C. Y. Chen, T. H. Wang and C. M. Ho, *Anal. Chem.*, 2004, **76**, 6908–6914.
35 Y. Xia and G. M. Whitesides, *Angew. Chem., Int. Ed.*, 1998, **37**, 550–575.
36 P. Monfort and B. Baleux, *J. Microbiol. Methods*, 1996, **25**, 79–86.
37 M. L. Y. Sin, V. Gau, J. C. Liao, D. A. Haake and P. K. Wong, *J. Phys. Chem. C*, 2009, **113**, 6561–6565.
38 J. Sakakibara and R. J. Adrian, *Exp. Fluids*, 1999, **26**, 7–15.
39 K. F. Hoettges, J. W. Dale and M. P. Hughes, *Phys. Med. Biol.*, 2007, **52**, 6001–6009.
40 Z. Wang, V. Gidwani, Z. Sun, D. D. Zhang and P. K. Wong, *J. Assoc. Lab. Autom.*, 2008, **13**, 243–248.
41 V. Gidwani, R. Riahi, D. D. Zhang and P. K. Wong, *Analyst*, 2009, **134**, 1675–1681.
42 D. Meserve, Z. Wang, D. D. Zhang and P. K. Wong, *Analyst*, 2008, **133**, 1013–1019.
43 K. E. Mach, R. Mohan, E. J. Baron, M. C. Shih, V. Gau, P. K. Wong and J. C. Liao, *The Journal of urology*, 2011, **185**, 148–153.